Journal of Engineering and Applied Sciences 11 (1): 17-22, 2016
ISSN: 1816-949X

Effects of Band Superposition on the Satellite Imagery of Aerosol Optical Depth over West Africa

[1]E. Emetere Moses, [2]M.l. Akinyemi and [2]O. Akin-Ojo
[1]Department of Physics, Covenant University Canaan Land, P.M.B. 1023, Otta, Nigeria
[2]Department of Material Science, Africa University of Science and Technology, Abuja, Nigeria

Abstract: Estimating the aerosol optical properties over an area has been challenging due to the propagated signal from or to the satellite sensor. We propose that aerosols layer is formed in the atmosphere via reflected signals to create multipath. This act makes the satellite sensors see the superposition of multiple copies of transmitted signal which affects aerosol measurement at the long run. One of the reliable remote sensing techniques for investigating aerosol optical depth is the Multi-angle Imaging Spectro Radiometer (MISR). The MISR reanalysis is performed at the native horizontal resolution of 2°/3° longitude by 0.5° latitude and at 72 levels up to 0.01 hPa. The accuracy of MISR was investigated using mathematical experimentation. The spectral resolution of the green spectral band of the MISR corresponds to four bands (i.e., 1, 2, 3 and 6) on the MODIS. This occurrence affirms the band superposition theorem enacted in this research. This phenomenon is responsible for the inability of satellite or ground sensors to effectively measure the vertical distribution of aerosol. Five evidences of the superposition effect on satellite sensor adaptation were shown.

Key words: MISR, spectral radiance, aerosol optical depth, band superposition, Nigeria

INTRODUCTION

The release of anthropogenic aerosol (Emetere, 2013a, b; 2014a) into the atmosphere had been condemned because of its role in climate change. However, the advantage of aerosol in the atmosphere can be found in the initiation of fixation events for balancing carbon and nitrogen content in the atmosphere. Observations of urban aerosol dynamics in coastal regions depends on convective outflow which are limited because of the sporadic convective activity and the aerosol exist from the Planetary Boundary Layer (PBL) to the free troposphere and beyond. Satellite observations of Carbon monoxide (CO) and Aerosol Optical Depth (AOD) are useful for mapping convective outflow (Yuan *et al*., 2011; Coakley *et al*., 1983). For example, satellite observations showed that aerosol regulates cloud microphysics and lightning; aerosol scatters and absorbs solar radiation; aerosol acts as cloud condensation nuclei; aerosol modifies atmospheric temperature structure; aerosol affects atmospheric electrification when the charge separation and lightning increases with concentration of Cloud Condensation Nuclei (CCN) up to the threshold of CCN>2000 cm^{-3}, etc. The persistent challenges before scientists is the accurate estimation of aerosol distribution, aerosol-cloud interactions, aerosols physical and chemical properties. The solution to this challenge begins with the accuracy of the measurement tool, e.g., satellite imageries.

One of the major challenges of estimating aerosol using satellite imagery is superposition. The superposition engenders from signals reflected by the aerosol layers to form multi copies of the transmitted signals. Effects of superposition in remotely sensed location are subtle because most fundamental calculation in satellite communication did not capture error generated by the sensors' adaptation during harsh atmospheric perturbations. In image processing, superposition is useful for blending types of imagery captured per time. However, during transmission of satellite signals to ground or vis-a-vis, the electromagnetic data has the tendency of superimposing. The superposition is due to the band peculiarity. Despite band-width demarcation, superposition may occur when electromagnetic data (from ground to satellite or vis-a-vis) faces multiple scattering when traveling through thick-moving layered aerosol. Hence, the possibility of a fundamental error may occur. In the typical West Africa coastal region, satellite observation of aerosol may be difficult to convert into a quantitative model because it is characterized by active photochemistry, rapid convective mixing along with lightning discharge, high humidity, widespread biomass burning and growing industrial emissions. The extended effect is the massive missing data within the satellite data set. Many reasons have been adduced to the causes of large missing satellite data. The Troposphere Column

Corresponding Author: E. Emetere Moses, Department of Physics, Covenant University Canaan Land, P.M.B. 1023, Otta, Nigeria

Ozone (TTOC) record derived from the NIMBUS-7 observations is the most extensive. However, the inability of NIMBUS-7 to measure accurately the vertical distribution of aerosol still remains its shortcoming. In this study, we studied the aerosol distribution on the MODIS and compared it with specific bands on MISR.

MISR operates at various directions i.e. nine different angles (70.5, 60, 45.6, 26.1, 0, 26.1, 45.6, 60, 20.5°) and gathers data in four different spectral bands (blue, green, red and near-infrared) of the solar spectrum. We compare the theories of the band spectra wavelength on the MISR and MODIS. We propose that the inability of the satellite remote sensing instruments to provide a broader estimate of aerosol optical properties over an area was not due to the quality of the satellite imagery (Kaufman *et al*., 2002) but, the fluctuating satellite sensor functionality due to poor sensor adaptation. The fluctuating satellite sensor functionality is initiated by band superposition. Unfortunately, no imaging enhancing technique has been able to detect this concept in practical terms.

Theoretical background: We propose that the aerosol optical depth is directly related to the atmospheric emissivity. We adopted the Palluconi and Meeks (1985), i.e.,:

$$LS_j = \left[\varepsilon_j L_j^{BB}(T) + (1-\varepsilon_j) L_j^{sky}\right]\tau_j + L_j^{atm} \quad (1)$$

Where:

Ls_j = The spectral radiance observed by the sensor
L_j^{BB} = The spectral radiance from a blackbody at surface Temperature T
L_j^{sky} = The spectral radiance incident upon the surface from the atmosphere
L_j^{atm} = The spectral radiance emitted by the atmosphere
ε_j = The surface emissivity at wavelength
ι_j = The spectral atmospheric transmission

The anomalies reported by numerous researchers on emissivity (Srivastava *et al*., 2010; Morgan, 2005) was summarized by the assumption that $L_j^{sky} \approx L_j^{atm}$:

$$LS_j = \varepsilon_j \tau_j L_j^{BB}(T) + (1+\tau_j - \varepsilon_j \tau_j) L_j^{atm} \quad (2)$$

From the Emetere (2014a), we assume that the total spectral radiance is not strictly dependent on the angular displacement of the sensor. Therefore, spectral radiance from a blackbody at surface temperature T is reduced to:

$$LS_j = \frac{R\Omega^A}{\pi}\int_{\lambda_1}^{\lambda_2} \varepsilon_j \tau_j g_j L_j^{BB}(\lambda, T)$$

Combining Eq. 2 and later equation gives the governing equation shown below:

$$\left(\frac{R_\Omega A}{\pi}\int_{\lambda_1}^{\lambda_2} g_j L_j^{BB}(\lambda, T)\right) - L_j^{BB}(T) = \frac{(1+\tau_j - \varepsilon_j \tau_j)}{\varepsilon_j \tau_j} L_j^{atm}$$

Where:

R_Ω = The impedance of satellite sensor (>10 MΩ)
A = The area covered by the sensor (typically 100×100 km scenes for ERS and 165×165 km for radarsat wide)
g = The responsivity of the sensor at different wavelengths (preferable 0.62 μm) (Emetere, 2014b)

$$L_j^{BB}(T) = \frac{C_1}{\lambda_j^s \pi\left[\exp\left(\frac{C_2}{\lambda_2 T}\right) - 1\right]} \quad (3)$$

Where:

C_1 = First radiation constant = 3.74151×10^{-16} (Wm^2)
C_2 = Second radiation constant = 0.0143879 (mK)

The relationship between LS_j and L_j^{atm} was calculated by the Temperature Polynomial Expansion Scheme (TPES) for earth radiation (Emetere, 2014c; Uno and Emetere, 2012). It is given as:

$$L_j^{atm} = \left(\frac{2}{3}\right)^n LS_j \quad (4)$$

At low visibility conditions, the radiance scattered by the atmospheric aerosols comprise of a large portion of the total radiance. This kind of total radiance can be equated to the angstrom parameter. The new transformation can be seen from equation (Srivastava *et al*., 2010; Omotosho *et al*., 2015):

$$\alpha = -\frac{d\ln\tau_a}{d\ln\lambda} \quad (5)$$

Where:

α = The angstrom parameter
ι_a = The aerosol optical depth
λ = The wavelength

$$\tau_a = -\lambda \exp\left(\frac{R_\Omega A}{\pi}\int_{\lambda_1}^{\lambda_2} g_j L_j^{BB}(\lambda, T)\right)$$

MATERIALS AND METHODS

Mathematical evidence of the satellite superposition theory: The thick layered moving aerosol forms different optical medium with an unknown refractive index. Hence, the possibility of having multiple refractive index can be seen in Fig 1. The satellite sensor is encountered by multi-angular refraction as shown in Fig 2.

From the basic of refractive index, we define the types of refractive indexes expected in Eq. 6:

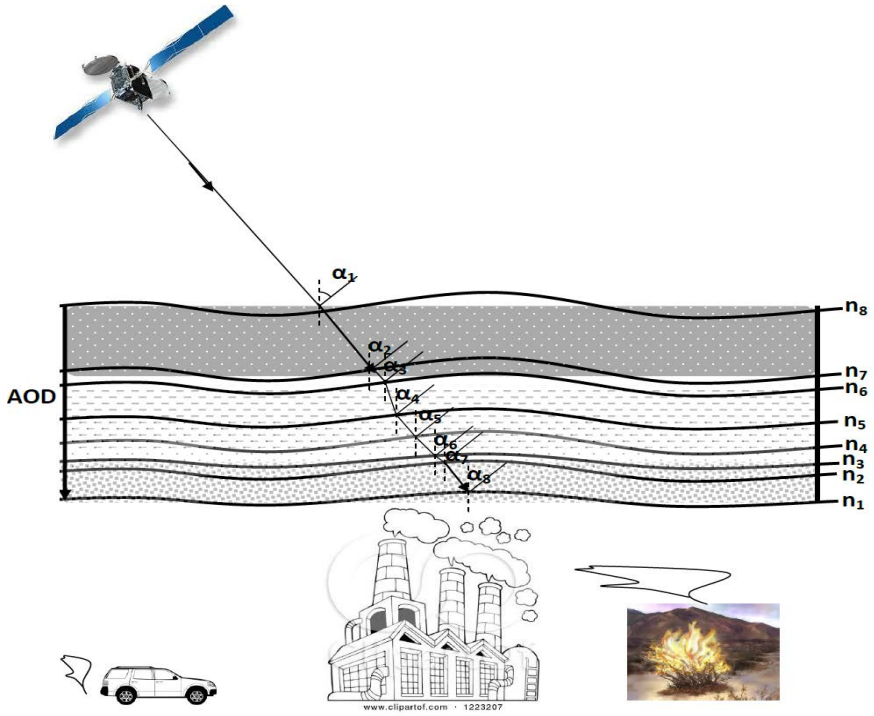

Fig. 1: Validation of atmospheric constants over regions

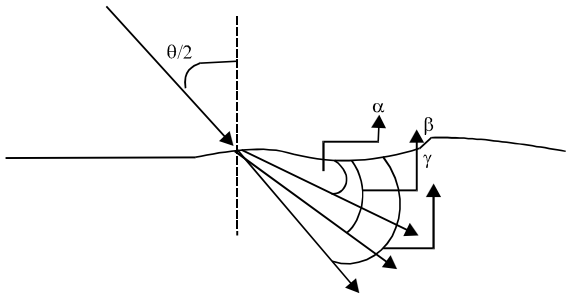

Fig. 2: Moving effect of aerosols on refractive indexes

$$\left.\text{Sin}\frac{\theta}{2}=n\cos\alpha,\ \text{Sin}\frac{\theta}{2}=n\cos\beta,\ \ \text{Sin}\frac{\theta}{2}=n\cos\gamma\right\} \quad (6)$$

When the total angle expected during data capture is considered, the basics of trigonometry:

$$\text{Sin}\theta=\left(\text{Sin}\frac{\theta}{2}+\sin\frac{\theta}{2}\right)\cos\frac{\theta}{2}$$

would be applied to Eq. 6 as:

$$\text{Sin}\theta=n\cos\alpha\cos\frac{\theta}{2}+n\cos\beta\cos\frac{\theta}{2}+n\cos\gamma\cos\frac{\theta}{2} \quad (7)$$

From the basic principle of the sun photometer, the relative air mass is given as:

$$m=\frac{1}{\sin(\theta)}$$

However, we assume that for the satellite sensor expressed in Fig. 2, the refractive index can be related to the pollution concentration as:

$$n=\frac{c}{\sin(\theta)} \quad (8)$$

Hence, if Eq. 8 is slotted into Eq. 7, the emerging results is given as:

$$C=n^2\cos\alpha\cos\frac{\theta_i}{2}+n^2\cos\beta\cos\frac{\theta_i}{2}+\cdots\ldots\ldots\ldots n^2\cos\gamma\cos\frac{\theta_n}{2} \quad (9)$$

The individual term of the right side of Eq. 9 is synonymous to the solution of a 3D dispersion model (Omotosho *et al*., 2015).

RESULTS AND DISCUSSION

Four bands, i.e., infrared, red, green and blue of the MISR was considered. The green band is unique because

Table 1: Corresponding MODIS bands in the MISR green band

Band width (nm)	L_j^{BB} (W m^{-2}) 10^{-9}	L_{j2}^{BB} (W m^{-2}) 10^{-9}	τ_a (μm)	τ_{a2} (μm)	Central wavelength (nm)
545-550	7.9192	21.560	0.5475	0.5475	547.50
545-555	11.5640	31.483	0.5500	0.5500	550.00
545-560	16.8280	45.813	0.5525	0.5525	552.50
545-565	24.4020	66.436	0.5550	0.5550	555.00

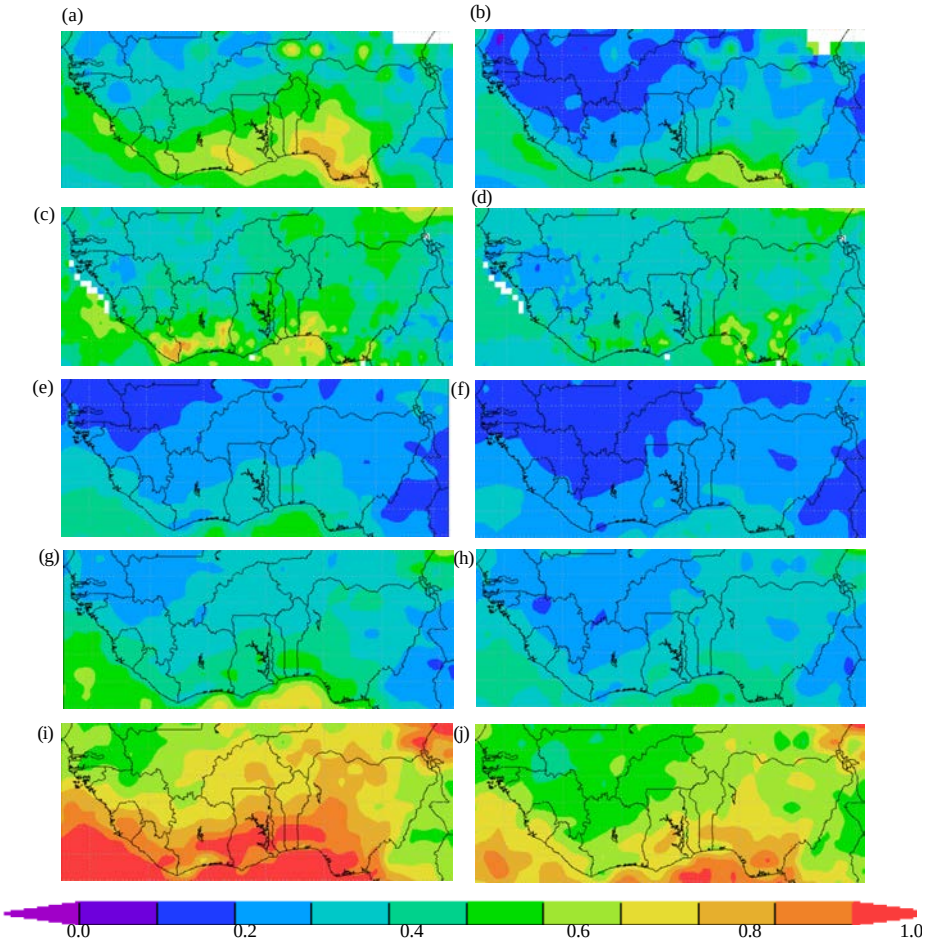

Fig. 3: a) AOD at λ = 550 nm, 2007; b) AOD at λ = 555 nm, 2007; c) AEOD at λ = 500 nm, 2007; d) AOD at λ = 388 nm, 2007; e) AEOD at λ = 388 nm, 2007; f) AOD at λ = 550 nm, 2013; g) AOD at λ = 555 nm, 2013; h) AEOD at λ = 500 nm, 2013; i) AEOD at λ = 388 nm, 2013; j) AOD at 388 nm, 2013

other bands. The corresponding spectra band on the MODIS was compared with the green spectra band on the MISR as shown in Table 1. We adopted the ERS scenes 100×100 km for spectral radiance L_j^{BB} and the Radarsat scenes 165×165 km for spectral radiance L_j^{BB}. We observe from our calculation that the green band of MISR intersect with four bands on the MODIS, i.e., first, second third and sixth bands Table 1. Fortunately, these intersected bands are located within the Land/Cloud/Aerosol boundaries and Land/Cloud/Aerosol properties.

Unlike the Optical Properties of Aerosols and Clouds (OPAC) and cirrus clouds models which operates at 61 wavelengths (between 0.25 and 40 μm) and 67 wavelengths (between 0.28 and 40 μm), respectively, we focused on the wavelengths 500, 550, 388 and 555 nm on the MISR to buttress on the Band superposition theory explained in Table 1 and Fig. 3a-j. The pictorial analysis for 2007 shown in Fig. 3a and b reveals a better NASA-Giovanni satellite sensitivity for AOD at a wavelength 550 nm than for Aerosol Extinction Optical Depth (AEOD) at a wavelength 550 nm. Also, the pictorial analysis shown in Fig. 3d ande reveals a better NASA-Giovanni satellite sensitivity for AEOD at a wavelength 388 nm than for AOD at a wavelength 388 nm. The AOD at a wavelength 500 nm Fig. 3c is less sensitive. In 2013, the satellite imagery Fig. 3f and j follows the same

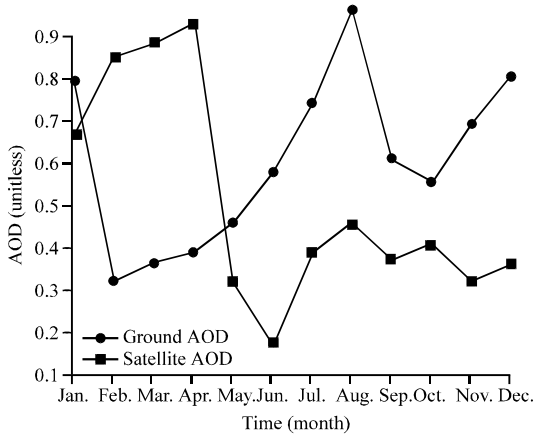

Fig. 4: Ground and Satellite measurement for Ilorin, Nigeria

feature shown in 2007. The trend is same within 2007-2013. The extended effect of sensor adaptation is clearer when the AERONET-aerosol optical depth ground data was compared with the satellite data set over Ilorin, Nigeria Fig. 4 for the year 2008. The disparity in both measurements may be trivially explained as the interference of clear and cloudy sky.

More technically, the superposition theory which we have proven numerically may be responsible for the major and minor defaults of satellite measurements.

We observed that no superposition occurred for two days, i.e., 10th Jan. and 20th April in 2008. These dates were obtained from the intersection between the ground and satellite data set. Recall that, the mathematical proof of the superposition concept of satellite sensors was explained earlier. The individual term on the right side of Eq. 9 is synonymous to the solution of a 3D dispersion model. This means that part of the satellite sensor adaptation may the relative motion between the moving aerosol layers in the atmosphere and the moving earth. That could also be one of the reasons the green band of MISR intersect with four bands on the MODIS.

CONCLUSION

In the study, we have been able to show via five evidences that the effect of superposition is enormous in affirming the accuracy of remotely sensed data set. First, we have been able to show that the green band spectra of the MISR captured the wavelengths of four different bands on the MODIS. Second, we have been able to show analytically that the relative motion between the moving aerosol layers in the atmosphere and the moving earth creates a multiple refractive index that dictates the superposition event. Third, we have been able to show that the TPES algorithm can be used to aid satellite imagery or passive ground sensors. The TPES is expected to determine the radiative progression. Recall that, we had explained that band superposition may be due to the differential radiation trapped amidst aerosol depth. This explanation is responsible for the inability of the passive ground sensors and satellite imagery to determine the vertical distribution of aerosol layers. Fourth, we showed evidences of band superposition theory via seven years aerosol optical depth data set of the coastal region of West Africa where harsh atmospheric perturbations are expected. Fifth, we showed evidence of band superposition via a comparative analysis of the ground and satellite ground stations. Hence, the need for the inclusion of the superposition term to regional climate models is essential to improve the accuracy of satellite exploration in recent times.

ACKNOWLEDGEMENTS

The satellite data was gotten from the Giovanni-NASA. Researcher appreciates the partial sponsorship of Covenant University.

REFERENCES

Coakley Jr., J.A., R.D. Cess and F.B. Yurevich, 1983. The effect of tropospheric aerosols on the Earth's radiation budget: A parameterization for climate models. J. Atmos. Sci., 40: 116-138.

Emetere, M.E., 2013a. Modeling of particulate radionuclide dispersion and deposition from a cement factory. Ann. Environ. Sci., 7: 71-77.

Emetere, M.E. and M.L. Akinyemi, 2013b. Modeling of generic air pollution dispersion analysis from cement factory. Analele Universitatii din Oradea-Seria Geografie, 23: 181-189.

Emetere, M.E., 2014a. Forecasting hydrological disaster using environmental thermographic modeling. Adv. Meteorol., Vol. 2014. 10.1155/2014/783718

Emetere, M.E., 2014b. Profiling laser-induced temperature fields for superconducting materials using mathematical experimentation. J. Thermophysics Heat Transfer, 28: 700-707.

Emetere, M.E., 2014c. Theoretical forecast of the health implications of citing nuclear power plant in Nigeria. J. Nuclear Particle Phys., 4: 87-93.

Kaufman, Y.J., D. Tanre and O. Boucher, 2002. A satellite view of aerosols in the climate system. Nature, 419: 215-223.

Morgan, J.A., 2005. Bayesian estimation for land surface temperature retrieval: The nuisance of emissivities. Geosci. Remote Sens. IEEE. Trans., 43: 1279-1288.

Omotosho, T.V., M.E. Emetere and O.S. Arase, 2015. Mathematical projections of air pollutants effects over Niger Delta region using remotely sensed satellite data. Intl. J. Appl. Environ. Sci., 10: 651-664.

Palluconi, F.D. and G.R. Meeks, 1985. Thermal Infrared Multispectral Scanner (TIMS): An Investigator's Guide to TIMS Data. Jet Propulsion Laboratory Publication, USA., Pages: 92.

Srivastava, P.K., T.J. Majumdar and A.K. Bhattacharya, 2010. Study of land surface temperature and spectral emissivity using multi-sensor satellite data. J. Earth Syst. Sci., 119: 67-74.

Uno, U.E. and M.E. Emetere, 2012. Analysing the impact of soil parameters on the sensible heat flux using simulated temperature curve model. Int. J. Phys. Res., 2: 1-9.

Yuan, T., L.A. Remer, K.E. Pickering and H. Yu, 2011. Observational evidence of aerosol enhancement of lightning activity and convective invigoration. Geophys. Res. Lett., Vol. 38, 10.1029/2010GL046052.